Research Square

Preprints are preliminary reports that have not undergone peer review.
They should not be considered conclusive, used to inform clinical practice,
or referenced by the media as validated information.

Discovery of Serum Biomarkers for Early Detection of Rabies Virus Infection Using Global Metabolic Profiling

Wongsakorn Wongwadhunyoo
Mahidol University
Phornpimon Tipthara
Mahidol University
Joel Tarning
University of Oxford
Punchaya Supasawat
Chulabhorn Royal Academy
Thassanee Srisook
Chulabhorn Royal Academy
Kunjimas Ketsuwan
Mahidol University
Rojjanaporn Pulmanausahakul
Chulabhorn Royal Academy
Woranich Hinthong
Chulabhorn Royal Academy
Promsin Masrinoul
Mahidol University
Onrapak Reamtong
Mahidol University
Peerut Chienwichai
peerut.chi@cra.ac.th

Chulabhorn Royal Academy

Article

Keywords: rabies virus, untargeted metabolomics, early biomarker, 5β-cholestane-3α,7α,12α,26-tetrol, cystathionine, glycocholic acid

Posted Date: May 19th, 2026

DOI: https://doi.org/10.21203/rs.3.rs-9323973/v1

License: This work is licensed under a Creative Commons Attribution 4.0 International License.
Read Full License

Additional Declarations: No competing interests reported.

Abstract

Rabies virus (RABV) infection is a fatal zoonotic disease for which early diagnosis remains a major challenge. Timely intervention before the onset of clinical symptoms is critical for patient survival; however, reliable biomarkers of preclinical RABV infection are lacking. The identification of metabolic alterations during early infection may facilitate the development of early diagnostic tools. Hence, the aim of this study was to screen for serum metabolite biomarkers of early-stage RABV infection using a mouse model and an untargeted metabolomics approach. Mice were intramuscularly infected with RABV, and serum samples were collected at two time points prior to the virus entering the brain and at clinical onset. Metabolites were extracted and analyzed via mass spectrometry-based metabolomics. More than 14,000 features were detected, and more than 3,000 of those features showed significant alterations at the different stages of infection. Pathway analysis revealed that these changes were associated with multiple biological pathways related to RABV infection, including energy metabolism and steroid hormone biosynthesis. Multivariate statistical analysis, integrating statistical significance and area under the receiver operating characteristic curve (AUROC) performance, identified 304 potential biomarkers with strong discriminatory power. We then focused on endogenous host-derived metabolites with high AUROC values. Among the decreasing metabolites, 5β-cholestane-3α,7α,12α,26-tetrol and phytosphingosine-1-phosphate showed consistent downward trends, and these molecules have been linked to viral infection or neuropathology. Cystathionine, glycocholic acid, and taurolithocholic acid displayed increasing trends with strong diagnostic performance, highlighting their potential as biomarkers of early RABV infection. Overall, this study revealed distinct serum metabolic signatures associated with RABV infection and identified several endogenous metabolites with high diagnostic potential. These findings provide a foundation for the development of targeted metabolite panels and diagnostic assays, as well as early surveillance, risk stratification, and timely clinical intervention strategies for RABV infection.

Introduction

Rabies virus (RBV) is the cause of lethal zoonosis with an almost 100% fatality rate in the absence of timely treatment. It is an enveloped, bullet-shaped virus with a negative-sense single-stranded RNA genome [1]. Globally, RABV is responsible for an estimated 60,000 human deaths each year, which are clustered in resource-limited regions of Asia and Africa [2]. Patients typically seek medical care only after clinical symptoms of RABV infection appear, at which point treatment is no longer effective [3–5]. Post-exposure prophylaxis (PEP) remains the only intervention capable of preventing death following exposure to a rabid animal, and timely administration is critical for survival [6]. However, many exposed individuals fail to receive PEP because of factors such as financial constraints and low risk perception [7]. Therefore, improved early diagnosis of RABV infection would not only support more effective clinical management but might also motivate at-risk individuals to promptly seek appropriate treatment.

The development of reliable diagnostic tools for RABV infection is challenging because of the unique biology of RABV. Infection typically begins when an animal harboring the virus—most commonly a dog—

bites a human and introduces virus-laden saliva into the wound [8]. The virus initially infects local myocytes and undergoes primary replication before entering peripheral nerves at the neuromuscular junction. After entering the nervous system, RABV travels retrogradely along axons toward the spinal cord and ultimately reaches the brain, where extensive inflammation develops and leads to fatal encephalitis [9, 10]. Given the neurotropic nature of RABV, and that it migrates through peripheral nerves to the central nervous system (CNS), viremia is generally absent in infected individuals; hence, the methods that are typically used to detect viral antigens in the blood are unreliable in the case of RABV infection [11].

The current gold standard for RABV detection is a fluorescent antibody test performed on brain tissue. However, this method is highly invasive and not feasible for antemortem diagnosis. To improve the practicality of detecting RABV in suspected cases, several diagnostic approaches have been explored using alternative types of clinical samples, for example serum or saliva [12]. In terms of the different methodologies that have been explored, direct rapid immunohistochemistry and the reverse transcription quantitative polymerase chain reaction (RT-qPCR) have demonstrated strong diagnostic performances, yet they are typically available only in specialized reference laboratories [12, 13]. Point-of-care lateral flow assays offer utility in field settings; however, they have a broad range of sensitivity (0%–62%), which limits their reliability in clinical decision-making [12, 13]. With these constraints, obtaining a thorough patient history is essential for an accurate diagnosis. Unfortunately, exposure to RABV is frequently overlooked, underreported, or forgotten, leading to missed or delayed recognition of RABV infection [14]. To address these challenges, a considerable volume of research has been conducted to identify novel biomarkers of RABV infection that would enable the early, reliable, and practical detection of the virus.

Pin et al. [15] subjected blood, saliva, and cerebrospinal fluid (CSF) samples from a patient clinically suspected of RABV infection to metagenomic next-generation sequencing (mNGS). Although prior tests for an RABV antigen, anti-RABV antibody, and viral isolation experiments were all negative, RABV-matched sequences were detected via mNGS in saliva approximately 25 days after exposure to rabid dogs, and in CSF at 43 days post-exposure; no viral sequences were identified in the tested blood samples. Similarly, Wu et al. [16] performed mNGS on blood and CSF samples from another suspected case, and they also obtained negative results from these specimens. However, metagenomic analysis of saliva samples revealed the presence of genes with 99.7% homology to the RABV nucleoprotein gene (RABV N gene), and RT-qPCR confirmed the infection. In an effort to develop more sensitive early-stage diagnostics, Ren et al. [17] evaluated a recombinase polymerase amplification–CRISPR nucleic acid assay and found that it could detect at least one copy of an RABV genomic RNA molecule as early as three days post-infection (dpi) in rat CSF. While CSF-based methods have demonstrated high sensitivity, CSF collection is impractical in standard clinical settings. In another study, Li et al. [18] utilized magnetic bead-based serum peptide profiling using matrix-assisted laser desorption/ionization time-of-flight mass spectrometry (MALDI-TOF MS) to identify biomarkers of early RABV and Irkut virus infections. They identified serum peptides with diagnostic potential at 2–8 dpi, achieving sensitivities above 85%. Furthermore, Yamada et al. [19] analyzed serum protein expression in RABV-infected mice and reported that apolipoprotein A1 was upregulated prior to the onset of neurological symptoms. ELISA results

validated and supported its potential as an early serum biomarker of RABV infection. Together, these findings indicate that detectable biomarkers of early RABV infection may exist.

Metabolomics has emerged as a powerful approach for identifying disease biomarkers, particularly biomarkers of viral infections. Previous studies have demonstrated its utility in distinguishing infection states and disease severity. For example, Borras et al. [20] identified metabolites such as lipoxin A4 and prostaglandin J2 as promising indicators of respiratory viral infections, including influenza, while Gómez-Archila et al. [21] found that serum metabolites—including lipoproteins, creatine/creatinine, and tyrosine—change across the stages of HIV infection. Similarly, Shen et al. [22] reported that serum metabolites, such as bilirubin products, kynurenine, and N-palmitoylsphingosine, can be used to classify severe COVID-19 cases with high accuracy. Despite these advances, metabolomics has not yet been applied to identify biomarkers of RABV infection, particularly during its early stages. To address this diagnostic gap, we employed global MS-based serum metabolite profiling in a mouse model of intramuscular RABV infection to detect metabolic alterations across stages of RABV infection. The aims of this study were to identify candidate biomarkers of early RABV infection and thus provide foundational knowledge for the future development of timely and precise diagnostic tools to improve clinical outcomes.

Methods

Ethical statement

All experiments involving animals were approved by the Faculty of Veterinary Science, Mahidol University-Animal Care and Use Committee (approval number: MUVS-2024-05-32). The procedures were strictly conducted according to the guidelines for the use of animals provided by the National Research Council of Thailand and complied with the ARRIVE guidelines. All protocols that involved the use of cells or virions were approved by Mahidol University (approval number: MU 2023-040).

Viral culture, animal husbandry, and RABV infection

The CVS-11 strain of RABV was provided by the Department of Medical Services, Ministry of Public Health, Thailand. Mouse neuroblastoma (Neuro-2a) cells (ATCC, VA, USA) were used to propagate the virus, and these were cultured using Eagle's Minimum Essential Medium supplemented with 10% fetal bovine serum and penicillin–streptomycin (Thermo Scientific, MA, USA). Viral titers were measured using an immunofluorescence assay, as previously described [23].

Two different types of animal experiments were performed in controlled ABSL-3 facility with *ad libitum* food and water. The first type was conducted to determine the clinical outcomes and their timing in mice administered RABV. For this, 10 female ICR mice (6–8 weeks old) (Nomura Siam International, Bangkok, Thailand) were transported, acclimatized for 7 days, and each intramuscularly infected with 10×10^5 Foci-Forming Unit (FFU) of RABV via the caudal thigh muscle under isoflurane anesthesia. The mice were observed daily for 14 days for clinical signs of RABV infection and assigned clinical scores using the definitions of Meslin et al. [24]. Mice with a clinical score of ≥3 (i.e., with at least a lack of hind-limb

coordination) were euthanized immediately with isoflurane inhalation followed by exsanguination via heart puncture. All remaining mice were euthanized at 14 dpi with the same protocol.

The second type of animal experiment was conducted to collect clinical samples at different stages of RABV infection. For this, sample size was calculated and a total of 24 female ICR mice (6–8 weeks old) were transported, acclimatized for 7 days, and randomly allocated to either a control group (n = 6) or an infection group (n = 18). The control group mice were injected with culture medium and immediately sacrificed. Serum and brain samples were then collected. The 18 mice in the infection group were inoculated with 10×10^5 FFU of RABV and monitored for 14 days by an experienced veterinarian. At 7 dpi, six mice with a clinical score of 1 (ruffled fur) were randomly selected and euthanized for sample collection; these mice formed the “early infection” group. At 14 dpi, six mice with a clinical score of 2 (tremor when held in the air) were randomly selected and euthanized; these mice formed the “late infection” group. Throughout the study period, mice with a clinical score of ≥3 were immediately euthanized; these mice formed the “clinical infection” group. All injections and euthanasia were performed under isoflurane inhalation and by isoflurane inhalation followed by exsanguination via cardiac puncture, respectively. The same sample collection procedures were used for the control and infection groups. Brain tissue samples were placed in TRIzol reagent (Merck, Darmstadt, Germany) and stored at −80°C until analysis. Similarly, serum samples were stored at −80°C until analysis. All procedures were performed by experienced veterinarians.

RT-qPCR for the detection of RABV infection

Brain tissue samples from all mice were analyzed for RABV N gene expression using RT-qPCR. Briefly, the total mRNA extracted from the samples was reverse-transcribed into complementary DNA (cDNA) using a RevertAid First Strand cDNA Synthesis Kit (Thermo Scientific). The RABV N gene (forward primer: AATCTCACCGCAAGGGAAGC; reverse primer: ATGCAGCAATAACCGTCGCA) was subsequently quantified using the Maxima SYBR Green qPCR Master Mix (Thermo Scientific) and CFX Opus Dx Real-Time PCR Detection System for IVD (Bio-Rad, CA, USA). Mouse glyceraldehyde 3-phosphate dehydrogenase (GAPDH; forward primer: CGTGCCGCCTGGAGAAACC; reverse primer: TGGAAGAGTGGGAGTTGCTGTTG) was used as the housekeeping gene. Relative expression levels were calculated using the $2^{-\Delta CT}$ method and compared across the experimental groups.

Metabolite extraction

All serum samples were processed for metabolite extraction in a single batch, following the method of Lu et al. [25]. In brief, 20 μL of serum was mixed with 80 μL of cold methanol and vortexed vigorously for 1 min. The mixture was then incubated at 4°C for 20 min and centrifuged at 12,000 rpm for 10 min. The resulting supernatant was transferred to a fresh tube and dried using a speed vacuum concentrator (Tomy Digital Biology, Tokyo, Japan). The dried metabolite extracts were stored at −80°C until analysis.

MS-based metabolite identification

Metabolomic profiling was performed using an ultra-high-performance liquid chromatography system (Agilent 1260 Quaternary Pump, 1260 High-Performance Autosampler, and 1290 Thermostatted Column Compartment SL; Agilent Technologies, CA, USA) coupled to a DuoSpray ion source with electrospray ionization and a quadrupole TOF mass spectrometer (TripleTOF 5600+; SCIEX, MA, USA).

For chromatographic separation, 0.1% formic acid in water served as mobile phase A, and 0.1% formic acid in acetonitrile served as mobile phase B. The dried metabolite extracts were reconstituted in a 1:1 (v/v) mixture of mobile phases A and B, transferred to liquid chromatography vials, and stored in the autosampler at 6°C. A 5 μL aliquot was injected in two technical replications onto a C18 reversed-phase column (ACQUITY UPLC BEH, 2.1 × 100 mm, 1.7 μm; Waters, MA, USA). Separation was conducted at 0.3 mL/min with the column maintained at 40°C. The gradient program began at 5% B and was held for 2 min (0.0–2.0 min), followed by increases to 60% B over 0.5 min (2.0–2.5 min), 80% B over 1.5 min (2.5–4.0 min), and 100% B over 8 min (4.0–12.0 min). The composition was held at 100% B for 5 min (12.0–17.0 min) and then decreased to 5% B over 0.1 min (17.0–17.1 min), with a 2.9 min re-equilibration period (17.1–20.0 min) before the next injection.

Data acquisition was performed using Analyst Software v1.7 (SCIEX). Metabolites were analyzed in both positive and negative ionization modes. An information-dependent acquisition method was used, consisting of a TOF MS survey scan followed by 10 dependent MS/MS scans in high-sensitivity mode with dynamic background subtraction. TOF MS scans covered *m/z* 100–1,000, and product ion scans covered *m/z* 50–1,000.

Quality control (QC) samples were prepared by pooling equal aliquots of all metabolite extracts. QC samples were injected at regular intervals—before, during, and after analytical runs—to monitor instrument stability and data quality.

Metabolite annotation

Metabolomic data acquired via LC–MS/MS (.wiff and .wiff.scan files) were converted to the Analysis Base File (.abf) format using the Reifycs ABF Converter (Reifycs, Tokyo, Japan). Metabolite annotation was conducted using MS-DIAL version 5.5 [26]. The detected features were annotated by applying the parameter settings optimized for soft ionization with chromatographic separation. The mass spectrometric method was data-dependent metabolomics, capturing both MS1 and MS/MS spectra. The mass accuracy thresholds were set at 0.01 Da for MS1 and 0.025 Da for MS2. Peaks were detected with a minimum height of 1,000 intensity units and a mass slice width >0.1 Da. The sigma window value for spectral deconvolution was set to 0.5, and no MS/MS abundance cutoff was applied.

Metabolites were identified by comparing our data with all public MS/MS metabolite databases, including 326,575 records for positive ion mode and 53,337 records for negative ion mode data. Retention time tolerance was set to 100 min, and accurate mass tolerances were set at 0.01 Da for MS1 and 0.025 Da for MS2. The common adduct ions were considered. For alignment, the retention time tolerance and MS1 tolerance were set to 0.1 min and 0.015 Da, respectively.

Data analysis and biomarker selection

The annotated metabolomic dataset was analyzed using the MetaboAnalyst online platform version 6.0 (https://www.metaboanalyst.ca/) [27]. Statistical analysis was performed using the Statistical Analysis [one factor] module. The peak intensities for all metabolomic features were filtered using the interquartile range based on the median intensity values. Subsequently, the data were normalized, transformed, and scaled using quartile normalization, cube-root transformation, and range scaling, respectively. To evaluate the reliability of the metabolite identification process, all data—including the QC sample data—were subjected to principal component analysis (PCA). High-quality datasets were defined by the clustering of QC samples at the center of the PCA plot [28]. Only datasets meeting this criterion were included in the downstream analyses.

For the exploratory data analysis, PCA was performed to assess the differences between the serum metabolomic data obtained from the control group and the experimental groups. A hierarchical clustering heatmap was generated to visualize the metabolic impacts of RABV infection across the different disease stages. The Euclidean distance measure and Ward clustering were applied. Significantly altered putative metabolites were identified based on a ≥2-fold change relative to the control group and an adjusted *p*-value of <0.05. These metabolites have been visualized using volcano plots, and the stage-specific metabolites are illustrated using an UpSet plot [29].

A pathway analysis was conducted to gain deeper insights into the metabolic pathway perturbations that occur during the different stages of RABV infection. All feature data—including the *m/z* values, ionization mode, *p*-values, and t-scores—were uploaded to the functional analysis module to generate peak-list profiles. Data from the positive and negative ionization modes were combined, and a mass tolerance of 5 ppm was applied. The Mummichog algorithm was used for high-throughput untargeted metabolomics analysis against the *Mus musculus* (Kyoto Encyclopedia of Genes and Genomes; KEGG) pathway library, with a significance threshold set at the top 10% of the peaks. The results are visualized using scatterplots.

To identify metabolic features with biomarker potential, orthogonal partial least squares–discriminant analysis (oPLS-DA) was performed to calculate variable importance in projection (VIP) scores. Candidate biomarkers were defined as metabolites that were significantly altered in an experimental group relative to the control group and had a VIP score >1. All selected features were further evaluated for their discriminative performance between the control and infection groups using the Biomarker Analysis module in MetaboAnalyst. Putative biomarkers with an area under the receiver operating characteristic curve (AUROC) >0.8 were determined to be potential serum biomarkers of RABV infection.

Results and discussion

Clinical signs of RABV infection were first observed four days after RABV inoculation

To establish a model of early RABV infection, mice (n = 10) were inoculated intramuscularly with RABV and monitored for disease progression over 14 days. The first clinical signs of RABV infection appeared at 5 dpi, and all mice exhibited symptoms by 10 dpi. By the end of the observation period, 70% of the mice had survived (Fig. S1). These results showed that the selected viral dose reliably induced clinical RABV infection in mice while allowing sufficient numbers of animals to remain for sampling at 14 dpi.

After establishing the conditions for the model of early RABV infection, we prepared two groups of mice: a control group (n = 6) and an infection group (n = 18). The mice in the control group were euthanized immediately after the start of the experiment. The mice in the infection group were inoculated with RABV and monitored for 14 days. During the observation period, two mice were found dead without preceding clinical signs of RABV infection and were therefore excluded from the analysis. The 16 remaining mice in the infection group were further divided into three groups based on their clinical scores: the early infection (n = 6), late infection (n = 6), and clinical infection (n = 4) groups (Fig. 1A).

To determine the disease stage at which the virus had reached the CNS, the point when the disease is considered incurable, brain tissue samples were collected from all mice, and RT-qPCR was utilized to detect the RABV N gene. As shown in Fig. 1B, this gene was detected in brain tissue samples from the clinical infection group only. This suggests that molecules that are altered in the early and late infection groups may serve as biomarkers of RABV infection prior to CNS invasion.

Most mouse models of RABV infection have comparable incubation periods and mortality rates. For example, Klein et al. [30] reported an incubation period of 7–13 dpi following intramuscular inoculation and survival rates of 0%–50% at 21 dpi, depending on the viral strain. Similarly, Yamada et al. [19] reported an incubation period of approximately 7 dpi. Notably, they demonstrated that RABV gradually spreads from the muscle to the spinal cord by 4 dpi, reaching the brain by 6 dpi, even before the onset of clinical symptoms. In comparison, in our study, four mice developed neurological signs at 4–7 dpi, while 12 mice displayed a slower progression to clinical RABV infection despite the absence of detectable RABV in the brain (Fig. 1). Because RABV infection is considered incurable once clinical symptoms appear [31, 32], the period before the virus reaches the brain is critical for timely therapeutic interventions. Therefore, we focused on identifying biomarkers present in the early and late infection groups.

Serum metabolites were altered prior to the detection of RABV in the brain

To determine whether the quantities of any serum metabolites differ during the stages of RABV infection and to identify any such metabolites, we extracted and identified metabolites from serum samples collected from the control group and the early, late, and clinical infection groups. Initially, QC procedures were performed according to predefined criteria, and tight clustering of QC samples was observed in the PCA plots generated from both positive and negative ion mode data. These results indicated that the MS-based methodology performed in a stable manner (Fig. S2).

Subsequently, a multivariate PCA was performed to visualize the differences between the groups' serum metabolite profiles. From the PCA score plot shown in Fig. 2A, it can be observed that the samples from the control group were tightly clustered, whereas the samples from the early infection group were widely distributed and partially overlapped with those of the control group. The samples from the late infection group overlapped with those from the control group and the early infection group. The samples from the clinical infection group were clearly separated from those of the control group and partially overlapped with those from the early and late infection groups. Notably, the greatest distinction was observed between the control and clinical infection groups. To validate these findings, we generated a hierarchical clustering heatmap to visualize the metabolite abundance patterns across the groups. The heatmap revealed distinct clustering between the control and infection groups (Fig. 2B). Together, these results indicate that RABV infection progressively induces substantial changes in the serum metabolome. Importantly, these alterations are detectable in the early stage of infection.

To date, only a few studies have been designed to identify changes in serum biomolecules during the early stages of RABV infection, and no study has specifically analyzed metabolites. Li et al. [18] reported alterations in serum peptides in RABV-infected mice as early as 1 dpi, which preceded the onset of clinical symptoms observed at 6–13 dpi. Although the identified peptide signatures achieved over 90% accuracy in discriminating RABV-infected mice from uninfected mice, the peptide sequences could not be recovered due to the low quality and quantity of the peptides, posing a major challenge for further diagnostic development. Interestingly, Yamada et al. [19] demonstrated that serum apolipoprotein A1 was upregulated during the incubation period of RABV infection and on the day of clinical onset. Moreover, it remained upregulated after low-dose RABV inoculation, although the sensitivity of detection was reduced. Together, these findings suggest that RABV infection can alter serum biomolecules during the preclinical stage of infection. Thus, we proceeded to screen for serum metabolites significantly altered at each stage of infection relative to the control group.

Among the 14,612 detected features, >3,000 were significantly altered across all infection stages (Table S1, Fig. S3). In the early infection group, 3,882 features showed significant differences, of which 1,521 could be assigned as putative metabolites (Fig. 3A, Table S2). The late infection group contained a slightly lower number of differing significant features (3,013), with 1,257 features annotated as metabolites (Fig. 3B, Table S3). The clinical infection group contained the highest number of significantly altered features (4,417), with 1,677 features annotated as metabolites (Fig. 3C, Table S4). When we examined the features that were consistently altered across all infection stages, 1,873 overlapping features were identified, of which 799 were annotated and considered putative metabolites.

The consistently altered metabolites were of particular interest because their abundances changed throughout the course of infection, making them potential indicators of each stage of RABV infection. The top five increased and decreased putative metabolites at all stages of RABV infection are presented in Table 1, and the top three increased and decreased metabolites are highlighted in Fig. 3A–C. Among these metabolites, several have been associated with viral infection or neuropathology. Indoline (2,3-dihydroindole), the hydrogenated form of indole—a metabolite within the tryptophan metabolic pathway

[33]—showed a 4–8-fold increase in abundance in the infected groups. Elevated levels of serum indoline have been reported in studies on biomarkers of non-small cell lung cancer [34]. In addition, alterations in indole and indole-derived metabolites have been documented following avian influenza virus infection [35] and in conditions associated with severe brain damage [36]. Furthermore, immune–CNS crosstalk [37], which is partly mediated by metabolic pathways that include the tryptophan metabolic pathway, may also be relevant in the context of RABV infection.

The metabolites C17-sphinganine and 1,2-didecanoyl-sn-glycero-3-phosphocholine were also significantly altered. C17-sphinganine is a sphingolipid component of the cell membrane that is reportedly altered in patients with sepsis and associated with inflammation, oxidative stress, and phospholipase activation, processes that can compromise membrane integrity and impair cellular function [38]. The glycerophospholipid 1,2-didecanoyl-sn-glycero-3-phosphocholine (PC(10:0/10:0)) is a major component of cell membranes. Alterations in phosphatidylcholine species with different fatty acid chains have been reported in patients with tick-borne encephalitis, which is caused by tick-borne encephalitis virus [39, 40]. Collectively, these findings suggest that the significantly altered putative metabolites identified in this study may contribute to the pathogenesis of RABV infection and thus provide insight into the progression of RABV infection.

Metabolic and stress hormone pathways were disrupted during RABV infection

Pathway analysis revealed that most of the changed metabolites were involved in metabolic pathways (Table S5). In the early infection group, lipid metabolic pathways were prominently enriched, including primary bile acid biosynthesis, linoleic acid metabolism, and amino acid metabolism (e.g., β-alanine metabolism) (Fig. 4A). Glycan metabolism (mannose-type O-glycan biosynthesis) and cofactor and vitamin (folate biosynthesis) metabolism were also enriched in the late infection group (Fig. 4B). In the clinical infection group, a broader range of pathways was enriched, including cysteine and methionine metabolism and lysine degradation (amino acid metabolism), fatty acid elongation and linoleic acid metabolism (lipid metabolism), and ubiquinone and other terpenoid–quinone biosynthesis and retinol metabolism (cofactor and vitamin metabolism) (Fig. 4C).

The few studies conducted on the early pathogenesis of RABV infection indicate that clinical infection is associated with widespread metabolic disturbances across multiple tissues. Zhao et al. [41] investigated metabolite alterations in the brains of RABV-infected mice and found significant changes in several amino acid-related pathways, including arginine, proline, alanine, aspartate, and glutamate metabolism, consistent with our findings. Similarly, Schutsky et al. reported alterations in energy-related metabolites in the brains of mice infected with RABV without prior immunization [42]. Furthermore, Obradović et al. examined serum metabolic parameters in RABV-infected mice and observed significant changes in energy-related metabolites, including glucose, cholesterol, and non-esterified fatty acids [43]. In the human context, O'Sullivan et al. conducted a metabolomic analysis of CSF samples from patients with RABV infection and found that metabolites involved in energy metabolism differed significantly between

survivors and fatal cases [44]. Collectively, these findings indicate that energy metabolism is disrupted during RABV infection and that this may contribute to disease progression.

In alignment with our findings, there are several reports of increased levels of stress hormones in RABV infection. We observed alterations in the steroid biosynthesis pathway throughout the course of infection, with steroid hormone biosynthesis enriched in the early and clinical infection groups (Table S5). Schutsky et al. [42] reported marked alterations in stress hormone levels in the brains of RABV-infected mice and a dramatic increase in serum corticosterone levels prior to the onset of clinical signs, a finding that mirrors the temporal pattern observed in our study. This observation is supported by Obradović et al.'s study, which showed elevated serum cortisol levels in mice that succumbed to RABV infection [43]. It has been hypothesized that the elevation of corticosterone represents a viral strategy to suppress host immune responses that might otherwise restrict viral spread. Together, these findings provide insight into the role that serum metabolic alterations play in the pathogenesis of RABV infection. In addition, they validate our strategy for identifying biomarkers of early-stage RABV infection.

Many of the potential biomarkers of RABV infection are host-derived metabolites

Multivariate discriminant analysis using oPLS-DA was applied to compare the dataset of each infection group with that of the control group. As shown in Fig. 5, the oPLS-DA models distinctly separated the control group from each infection group (early infection group: $R^2X = 0.36$, $R^2Y = 0.71$, $Q^2 = 0.68$ [Fig. 5A]; late infection group: $R^2X = 0.25$, $R^2Y = 0.56$, $Q^2 = 0.53$ [Fig. 5C]; clinical infection group: $R^2X = 0.50$, $R^2Y = 0.93$, $Q^2 = 0.89$ [Fig. 5E]). Subsequently, VIP scores were calculated for each metabolic feature to identify those with potential diagnostic relevance to RABV infection. Metabolic features with VIP scores >1 were selected (Tables S2–S4). The features that intersected across all stages of infection were then screened, and the top-ranking features (based on VIP scores) were visualized using S-plots derived from the oPLS-DA models, in which discriminant variables were expected to localize at the extremes of the plots (Table 2; Fig. 5B, D, F). The three putative metabolites that consistently exhibited high VIP scores across all infection stages were melophlin B/C/G/K/L/N/O, 5β-cholestane-3α,7α,12α,26-tetrol, and phytosphingosine-1-phosphate. These metabolites were located at the extremes of the S-plots generated for the early and clinical infection groups, whereas they shifted slightly toward the center in the S-plot generated for the late infection group, indicating modestly lower, yet still significant, VIP scores >1.

The multivariate oPLS-DA model is widely used in metabolomic studies to screen metabolic features with diagnostic potential. Its popularity in biomarker discovery arises from its interpretability and ability to identify metabolites contributing to group discrimination through VIP scores [45]. For example, Ranaraja et al. performed oPLS-DA to identify serum biomarkers of early-stage *Escherichia coli* infection in broiler chickens and subsequently identified robust candidate metabolites for further biomarker development [46]. Similarly, Li et al. used oPLS-DA to identify biomarkers of sepsis, reporting that metabolites with VIP scores >1 demonstrated good predictive performance, with AUROC values ranging from 0.8 to 0.9 [47]. In the present study, 304 putative metabolites were identified as potential

biomarkers of RABV infection using the criteria of significant differential abundance, a VIP score >1 across all infection stages, and an AUROC value >0.8 (Table S6).

We focused on endogenous host-derived metabolites rather than exogenous compounds that may be influenced by dietary intake or consumption rate. Based on the AUROC results, the top three decreasing candidate biomarkers were 5β-cholestane-3α,7α,12α,26-tetrol, phytosphingosine-1-phosphate, and 3aH-cyclopenta[a]chrysene-3a-carboxylic acid, 1-acetyleicosahydro-9-hydroxy-5a,5b,8,8,11a-pentamethyl-, (1R,3aS,5aR,5bR,9S,11aR). Likewise, the top three increasing candidate biomarkers were cystathionine, glycocholic acid, and taurolithocholic acid (Fig. 6).

Among the decreasing metabolites, 5β-cholestane-3α,7α,12α,26-tetrol yielded the highest AUROC value and exhibited a consistent declining trend following RABV infection (Fig. 6A). This metabolite is an intermediate in the conversion of cholesterol to cholic acid and is part of the primary bile acid biosynthesis pathway [48]. Reduced levels of 5β-cholestane-3α,7α,12α,26-tetrol have been reported in tissues of mice infected with *Toxoplasma gondii*, a neuroinvasive protozoan. Specifically, Chen et al. observed a significant decrease in this metabolite in the spleen of *T. gondii*-infected mice [49], while Ma et al. reported alterations in the hippocampus of such mice [50]. Both studies proposed this compound as a biomarker of *T. gondii* infection. Given that both *T. gondii* and RABV primarily target the CNS, it is plausible that changes in 5β-cholestane-3α,7α,12α,26-tetrol may also reflect early-stage RABV infection. Phytosphingosine-1-phosphate also showed a consistent decreasing trend across all infection groups (Fig. 6B). This phosphosphingolipid is involved in sphingolipid and glycerophospholipid metabolism in yeasts and mammals [51]. Altered levels of phytosphingosine-1-phosphate have been reported in the mesencephalon of mice in a Parkinson's disease model, and it has been proposed as a potential biomarker of Parkinson's disease [52]. The third metabolite with a decreasing trend was 3aH-cyclopenta[a]chrysene-3a-carboxylic acid, 1-acetyleicosahydro-9-hydroxy-5a,5b,8,8,11a-pentamethyl-, (1R,3aS,5aR,5bR,9S,11aR) (Fig. 6C). This is the first time that this molecule has been identified as a potential disease biomarker. Therefore, further investigation of its role in RABV infection and disease biomarker potential is warranted.

Regarding the increasing putative metabolites, cystathionine recorded the highest AUROC value (Fig. 6D). Cystathionine is a sulfur-containing amino acid derivative that is typically present at higher concentrations in the brain than in other tissues [53]. Its synthesis from serine and homocysteine is catalyzed by cystathionine β-synthase, and its subsequent conversion to cysteine is catalyzed by cystathionine γ-lyase; cysteine is a key regulator of cellular redox homeostasis [54]. RABV infection has been reported to induce cellular oxidative stress as part of its pathogenic mechanism [55, 56]. Therefore, the observed altered serum cystathionine levels may reflect metabolic changes associated with disease progression. Notably, changes in cystathionine levels have been reported in cerebral pathologies [57, 58], and cystathionine γ-lyase has been implicated in hepatitis B virus-related liver disease [59]. Together, these findings highlight the potential of cystathionine as a biomarker of early RABV infection.

Glycocholic acid and taurolithocholic acid ranked second and third, respectively, in the list of increasing metabolites with high AUROC values (Fig. 6E–F). Both compounds are conjugated bile acids: Glycocholic acid is formed by the conjugation of glycine to cholic acid, whereas taurolithocholic acid results from the conjugation of taurine to lithocholic acid. In addition to their established roles in digestion, bile acid conjugates act as signaling molecules capable of binding to receptors in the CNS, thereby contributing to the development of neurological disorders [60]. For example, glycocholic acid has been identified as a potential plasma biomarker of non-progressive outcomes after ischemic stroke and as a predictor of acute stroke prognosis [61], as well as a serum biomarker for the accurate detection and timing of traumatic brain injury [62]. Regarding taurolithocholic acid, elevated levels were observed in patients infected with severe fever with thrombocytopenia syndrome virus who had a low fatality rate, and it was hypothesized to mitigate host inflammatory responses during infection [63]. Collectively, these findings suggest that alterations in the abundance of glycocholic acid and taurolithocholic acid may be associated with certain stages of RABV infection.

This study contributes to the growing body of research focused on identifying early biomarkers of RABV infection. By combining metabolite profiling with multiple data analysis strategies, the study enabled the identification of novel disease-associated biomarkers with potential applicability for future diagnostic development. Nevertheless, several limitations of this study should also be acknowledged. First, the metabolite annotation process was primarily based on MS-derived features and database matching; therefore, some compounds were putatively identified. Authentic standards and targeted quantitative assays should be used to confirm the identity of these compounds. Second, this study was conducted using a murine model of RABV infection. Thus, the translational relevance of our findings to human RABV infection should be validated using clinical samples. Third, the small sample size of each group may have affected the statistical power and increased the risk of false positives, despite the use of multivariate analyses and AUROC evaluations. Finally, the detected serum metabolite alterations may have been due to systemic responses to infection, such as inflammation or metabolic stress, rather than RABV-specific effects. Therefore, further research is required to determine whether the alterations are specific for RABV infection.

Conclusion

In this study, we comprehensively characterized the serum metabolomic alterations that occur during RABV infection in a murine model and identified host-derived metabolites that increase or decrease in abundance prior to clinical onset. Several endogenous metabolites, particularly those with strong discriminatory performance (e.g., 5β-cholestane-3α,7α,12α,26-tetrol and cystathionine) were identified as potential biomarkers of early-stage RABV infection. The observed changes suggest that energy metabolism and steroid hormone synthesis are disrupted during disease progression. Collectively, these findings improve our understanding of host metabolic responses to RABV infection and support the utility of serum metabolomics for the early detection of RABV infection. Targeted quantitative analyses and studies with clinical samples are needed to determine the robustness and translational applicability of these candidate biomarkers of RABV infection.

Declarations

Acknowledgments

We express our sincere gratitude to the Department of Medical Sciences, Ministry of Public Health, Thailand, for providing the CVS-11 RABV strain used in this study. We also thank the staff of the Monitoring and Surveillance Center for Zoonotic Diseases in Wildlife and Exotic Animals, Faculty of Veterinary Science, Mahidol University, for providing access to the BSL-3 facility and for conducting the necessary training. We are grateful to Mr. Iyacoob Khunsri and Ms. Sanjira Jantarapornchai from the Center for Vaccine Development, Institute of Molecular Biosciences, Mahidol University, for their assistance with the virus preparation. We also thank Ms. Chonchanok Yingpaiboon for her help in preparing the figures. We thank Dr. Kristen Sadler from Scribendi (www.scribendi.com) for editing a draft of this manuscript.

Funding

This research project was supported by Chulabhorn Royal Academy (Fundamental Fund: fiscal year 2023 by National Science Research and Innovation Fund [FRB660044/0240 Project code 180859]).

Author contribution

R.P., P.M., and P.C. conceptualized and designed the study. W.W., P.T., P.S., T.S., K.K., and P.C. conducted experiments. W.W., P.T., J.T., O.R., and P.C. curated data. W.H., P.C. analyzed, interpreted and visualized data. W.W., P.T., J.T., and P.M. provided resources. R.P., P.M., and P.C. administered the project. P.C. acquired funding. W.W., R.P. and P.C. drafted the initial manuscript. All authors participated in reviewing the manuscript.

Data availability

The data that support the findings of this study are available in the supplementary material of this article.

Competing Interests Statement

The authors declare no competing interests.

References

1. Schnell, M. J., McGettigan, J. P., Wirblich, C. & Papaneri, A. The cell biology of rabies virus: using stealth to reach the brain. *Nat. Rev. Microbiol.* **8**, 51–61; 10.1038/nrmicro2260 (2010).
2. Hampson, K. et al. Estimating the global burden of endemic canine rabies. *PLoS Negl. Trop. Dis.* **9**, e0003709; 10.1371/journal.pntd.0003709 (2015).

3. Dhayhi, N. S. et al. First confirmed case of local human rabies in Saudi Arabia. *Int. J. Infect. Dis.* **87**, 117–118; 10.1016/j.ijid.2019.08.011 (2019).
4. Amoako, Y. A. et al. Rabies is still a fatal but neglected disease: a case report. *J. Med. Case Rep.* **15**, 575; 10.1186/s13256-021-03164-y (2021).
5. Amaral Mali, M. et al. The first confirmed human case of rabies, Timor-Leste, 2024. *Euro Surveill.* **29**, 2400241; 10.2807/1560-7917.ES.2024.29.18.2400241 (2024).
6. Haradanhalli, R. S., Fotedar, N., Kumari, N. & Narayana, D. H. A. Safety and clinical efficacy of human rabies immunoglobulin in post exposure prophylaxis for category III animal exposures. *Hum. Vaccin. Immunother.* **18**, 2081024; 10.1080/21645515.2022.2081024 (2022).
7. Changalucha, J. et al. The need to improve access to rabies post-exposure vaccines: lessons from Tanzania. *Vaccine* **37**, A45–A53; 10.1016/j.vaccine.2018.08.086 (2019).
8. Pieracci, E. G. et al. Vital signs: trends in human rabies deaths and exposures - United States, 1938–2018. *MMWR Morb. Mortal. Wkly Rep.* **68**, 524–528; 10.15585/mmwr.mm6823e1 (2019).
9. Hemachudha, T., Ugolini, G., Wacharapluesadee, S., Sungkarat, W. & Shuangshoti, S. Human rabies: neuropathogenesis, diagnosis, and management. *Lancet Neurol.* **12**, 498–513; 10.1016/S1474-4422(13)70038-3 (2013).
10. Fisher, C. R., Streicker, D. G. & Schnell, M. J. The spread and evolution of rabies virus: conquering new frontiers. *Nat. Rev. Microbiol.* **16**, 241–255; 10.1038/nrmicro.2018.11 (2018).
11. Sitprija, V. et al. Does contact with urine and blood from a rabid dog represent a rabies risk? *Clin. Infect. Dis.* **37**, 1399–1400; 10.1086/379130 (2003).
12. Ashwini, M. A. et al. Laboratory diagnosis of rabies in an endemic country: progress and challenges on the path to elimination. *Diagn. Microbiol. Infect. Dis.* **114**, 117123; 10.1016/j.diagmicrobio.2025.117123 (2026).
13. Lodha, L., Ananda, A. M. & Mani, R. S. Advancing rabies diagnosis: time for a new “gold standard”? *Mol. Diagn. Ther.* **29**, 153–159; 10.1007/s40291-024-00758-2 (2025).
14. Khadra, M. N. et al. From initial suspicion to accurate diagnosis: unmasking rabies in a case of suspected Guillain-Barre syndrome. *BMC Pediatr.* **25**, 648; 10.1186/s12887-025-05994-x (2025).
15. Pin, L., Lutao, X., Linjie, L., Qunjie, P., Weijun, F. & Wang, D. A new choice for human rabies diagnosis: a case report of metagenomics next-generation sequencing in diagnosis of human rabies. *J. Infect. Public Health* **15**, 1276–1278; 10.1016/j.jiph.2022.10.003 (2022).
16. Wu, J. et al. Metagenomic next-generation sequencing for etiological diagnosis of an unexpected rabies case with unclear exposure history. *BMC Infect. Dis.* **25**, 258; 10.1186/s12879-025-10687-y (2025).
17. Ren, M. et al. Early diagnosis of rabies virus infection by RPA-CRISPR techniques in a rat model. *Arch. Virol.* **166**, 1083–1092; 10.1007/s00705-021-04970-x (2021).
18. Li, N. et al. Early diagnosis of Irkut virus infection using magnetic bead-based serum peptide profiling by MALDI-TOF MS in a mouse model. *Int. J. Mol. Sci.* **15**, 5193–5198;

10.3390/ijms15045193 (2014).

19. Yamada, K. et al. Validation of serum apolipoprotein A1 in rabies virus-infected mice as a biomarker for the preclinical diagnosis of rabies. *Microbiol. Immunol.* **65**, 438–448; 10.1111/1348-0421.12929 (2021).
20. Borras, E. et al. Exhaled breath biomarkers of influenza infection and influenza vaccination. *J. Breath Res.* **15**, 046004; 10.1088/1752-7163/ac1a61 (2021).
21. Gómez-Archila, L. G. et al. Plasma metabolomics by nuclear magnetic resonance reveals biomarkers and metabolic pathways associated with the control of HIV-1 infection/progression. *Front. Mol. Biosci.* **10**, 1204273; 10.3389/fmolb.2023.1204273 (2023).
22. Shen, B. et al. Proteomic and metabolomic characterization of COVID-19 patient sera. *Cell* **182**, 59–72.e15; 10.1016/j.cell.2020.05.032 (2020).
23. Chienwichai, P. et al. Proteomic and phosphoproteomic analysis of rabies pathogenesis in the clinical canine brain and identification of a kinase inhibitor as a potential repurposed antiviral agent. *PLoS One* **20**, e0323931; 10.1371/journal.pone.0323931 (2025).
24. Meslin, F. X., Kaplan, M. M. & Koprowski, H. *Laboratory techniques in rabies.* 4th ed. World Health Organization (1996).
25. Lu, K. et al. Arsenic exposure perturbs the gut microbiome and its metabolic profile in mice: an integrated metagenomics and metabolomics analysis. *Environ. Health Perspect.* **122**, 284–291; 10.1289/ehp.1307429 (2014).
26. Tsugawa, H. et al. MS-DIAL: data-independent MS/MS deconvolution for comprehensive metabolome analysis. *Nat. Methods* **12**, 523–526; 10.1038/nmeth.3393 (2015).
27. Pang, Z. et al. MetaboAnalyst 6.0: towards a unified platform for metabolomics data processing, analysis and interpretation. *Nucleic Acids Res.* **52**, W398–W406; 10.1093/nar/gkae253 (2024).
28. Godzien, J. et al. Controlling the quality of metabolomics data: new strategies to get the best out of the QC sample. *Metabolomics* **11**, 518–528; 10.1007/s11306-014-0712-4 (2015).
29. Khan, A. & Mathelier, A. Intervene: a tool for intersection and visualization of multiple gene or genomic region sets. *BMC Bioinformatics* **18**, 287; 10.1186/s12859-017-1708-7 (2017).
30. Klein, A. et al. Comparative pathogenesis of different phylogroup I bat lyssaviruses in a standardized mouse model. *PLoS Negl. Trop. Dis.* **16**, e0009845; 10.1371/journal.pntd.0009845 (2022).
31. Davis, B. M., Rall, G. F. & Schnell, M. J. Everything you always wanted to know about rabies virus (but were afraid to ask). *Annu. Rev. Virol.* **2**, 451–471; 10.1146/annurev-virology-100114-055157 (2015).
32. Lacy, M. et al. Human rabies treatment-from palliation to promise. *Viruses* **16**, 160; 10.3390/v16010160 (2024).
33. Sorgdrager, F. J. H. et al. Tryptophan metabolism in inflammaging: from biomarker to therapeutic target. *Front. Immunol.* **10**, 2565; 10.3389/fimmu.2019.02565 (2019).
34. Han, Y. et al. Biomarkers for non-small cell lung cancer risk using multi-omics approaches: a nested case-control study. *Transl. Lung Cancer Res.* **14**, 3645–3658; 10.21037/tlcr-2025-603 (2025).

35. Mao, S. et al. Untargeted metabolomics reveals distinct serum metabolic profiles in avian influenza occupational exposure populations. *Metabolites* **15**, 663; 10.3390/metabo15100663 (2025).
36. Sobolev, P. D. et al. A sensitive method for the profiling of phenyl- and indole-containing metabolites in blood serum and cerebrospinal fluid samples. *J. Pharm. Biomed. Anal.* **260**, 116803; 10.1016/j.jpba.2025.116803 (2025).
37. Stone, T. W. & Williams, R. O. Tryptophan metabolism as a 'reflex' feature of neuroimmune communication. *J. Neurochem.* **168**, 3333–3357; 10.1111/jnc.16015 (2024).
38. Peng, J. et al. Serum metabolite profiling reveals metabolic characteristics of sepsis patients. *BMC Med. Genomics* **16**, 224; 10.1186/s12920-023-01666-w (2023).
39. Du, Y. et al. Insights into the molecular basis of tick-borne encephalitis from multiplatform metabolomics. *PLoS Negl. Trop. Dis.* **15**, e0009172; 10.1371/journal.pntd.0009172 (2021).
40. Du, Y. et al. Proteomic and metabolomic analysis of the serum of patients with tick-borne encephalitis. *J. Proteomics* **298**, 105111; 10.1016/j.jprot.2024.105111 (2024).
41. Zhao, P. et al. Characterization of small metabolites alteration in mice brain tissues after infected by rabies virus. *Infect. Genet. Evol.* **85**, 104571; 10.1016/j.meegid.2020.104571 (2020).
42. Schutsky, K. et al. Limited brain metabolism changes differentiate between the progression and clearance of rabies virus. *PLoS One* **9**, e87180; 10.1371/journal.pone.0087180 (2014).
43. Obradović, N. et al. Blood metabolic and hematology parameters and survivorship in mice after application of the rabies challenge virus standard. *Acta Sci. Vet.* **49**, 1794; 10.22456/1679-9216.111103 (2021).
44. O'Sullivan, A. et al. Metabolomics of cerebrospinal fluid from humans treated for rabies. *J. Proteome Res.* **12**, 481–490; 10.1021/pr3009176 (2013).
45. Anwardeen, N. R. et al. Statistical methods and resources for biomarker discovery using metabolomics. *BMC Bioinformatics* **24**, 250; 10.1186/s12859-023-05383-0 (2023).
46. Ranaraja, A. et al. Temporal metabolomic fingerprinting identifies adenine as a novel biomarker. *Sci. Rep.* **15**, 31580; 10.1038/s41598-025-16873-x (2025).
47. Li, Y., Wang, C. & Chen, M. Metabolomics-based study of potential biomarkers of sepsis. *Sci. Rep.* **13**, 585; 10.1038/s41598-022-24878-z (2023).
48. Cronholm, T. & Johansson, G. Oxidation of 5β-cholestane-3α, 7α, 12α-triol by rat liver microsomes. *Eur. J. Biochem.* **16**, 373–381; 10.1111/j.1432-1033.1970.tb01091.x (1970).
49. Chen, X. Q. et al. Profiling of the perturbed metabolomic state of mouse spleen during acute and chronic toxoplasmosis. *Parasit. Vectors* **10**, 339; 10.1186/s13071-017-2282-6 (2017).
50. Ma, J. et al. Toxoplasma gondii induces metabolic disturbances in the hippocampus of BALB/c mice. *Parasitol. Res.* **120**, 2805–2818; 10.1007/s00436-021-07222-8 (2021).
51. Kondo, N. et al. Identification of the phytosphingosine metabolic pathway leading to odd-numbered fatty acids. *Nat. Commun.* **5**, 5338; 10.1038/ncomms6338 (2014).

52. Li, X. Z. et al. Cerebral metabonomics study on Parkinson's disease mice treated with extract. *Phytomedicine* **20**, 1219–1229; 10.1016/j.phymed.2013.06.002 (2013).
53. Cooper, A. J. The role of glutamine transaminase K in metabolism. *Neurochem. Int.* **44**, 557–577; 10.1016/j.neuint.2003.12.002 (2004).
54. Zuhra, K. et al. Cystathionine-β-synthase: molecular regulation and pharmacological inhibition. *Biomolecules* **10**, 697; 10.3390/biom10050697 (2020).
55. Jackson, A. C. et al. Role of oxidative stress in rabies virus infection. *Adv. Virus Res.* **79**, 127–138; 10.1016/B978-0-12-387040-7.00008-1 (2011).
56. Chienwichai, P. & Reamtong, O. Application of multi-omics technologies to decipher rabies pathogenesis. *Thai J. Vet. Med.* **50**, 129–136; 10.56808/2985-1130.3010 (2020).
57. Amano, H. et al. Cystathionine as a potential urinary marker. *Cancer Sci.* **116**, 3102–3112; 10.1111/cas.70169 (2025).
58. Branzoli, F. et al. In vivo detection of cystathionine in brain tumors. *Magn. Reson. Med.* **82**, 1259–1265; 10.1002/mrm.27810 (2019).
59. Jin, C. et al. Cystathionine gamma-lyase as an inflammatory factor. *Sci. Rep.* **15**, 17777; 10.1038/s41598-025-98922-z (2025).
60. Grant, S. M. & DeMorrow, S. Bile acid signaling in neurological disorders. *Int. J. Mol. Sci.* **21**, 5982; 10.3390/ijms21175982 (2020).
61. Wu, M. H. et al. Identification of a potential prognostic plasma biomarker. *Proteomics Clin. Appl.* **17**, e2200081; 10.1002/prca.202200081 (2023).
62. Zhang, G. et al. Plasma metabolome to identify biomarkers in traumatic brain injury. *Neuroreport* **32**, 415–422; 10.1097/WNR.0000000000001576 (2021).
63. Zheng, X. et al. Taurolithocholic acid protects against viral haemorrhagic fever. *Nat. Microbiol.* **9**, 2583–2599; 10.1038/s41564-024-01801-y (2024).

Figures

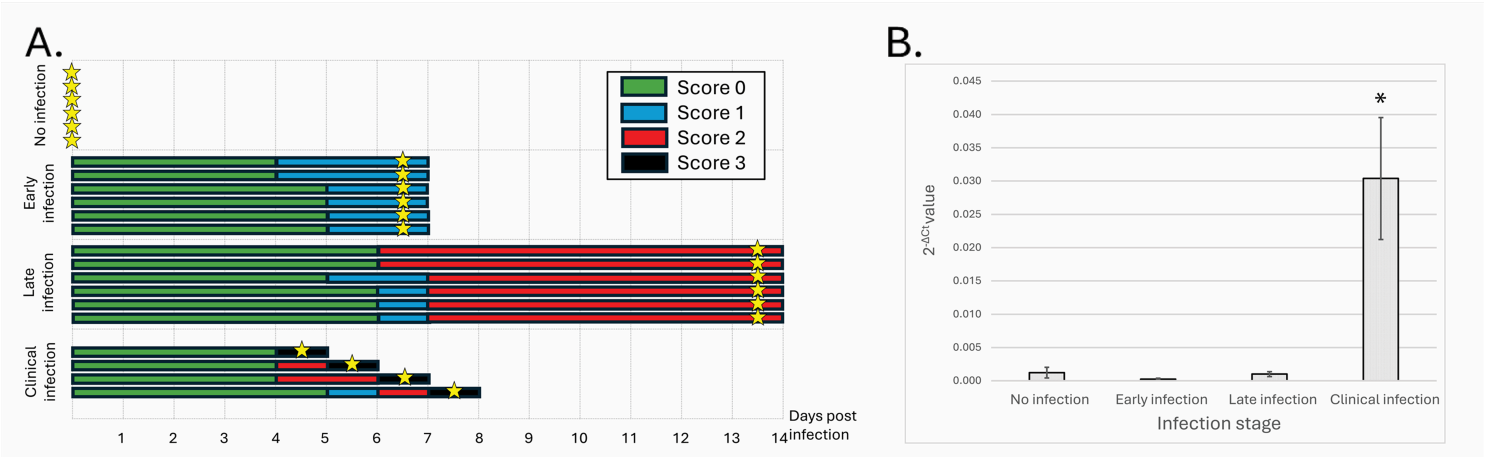


Figure 1

Clinical symptoms and confirmation of RABV infection in mice injected with RABV. A. Bar graph showing the clinical scores of each mouse over time. Yellow stars: date of euthanasia. B. The RABV N gene levels detected in brain tissue samples taken from each group. * indicates $p < 0.05$. Error bars represent standard error.

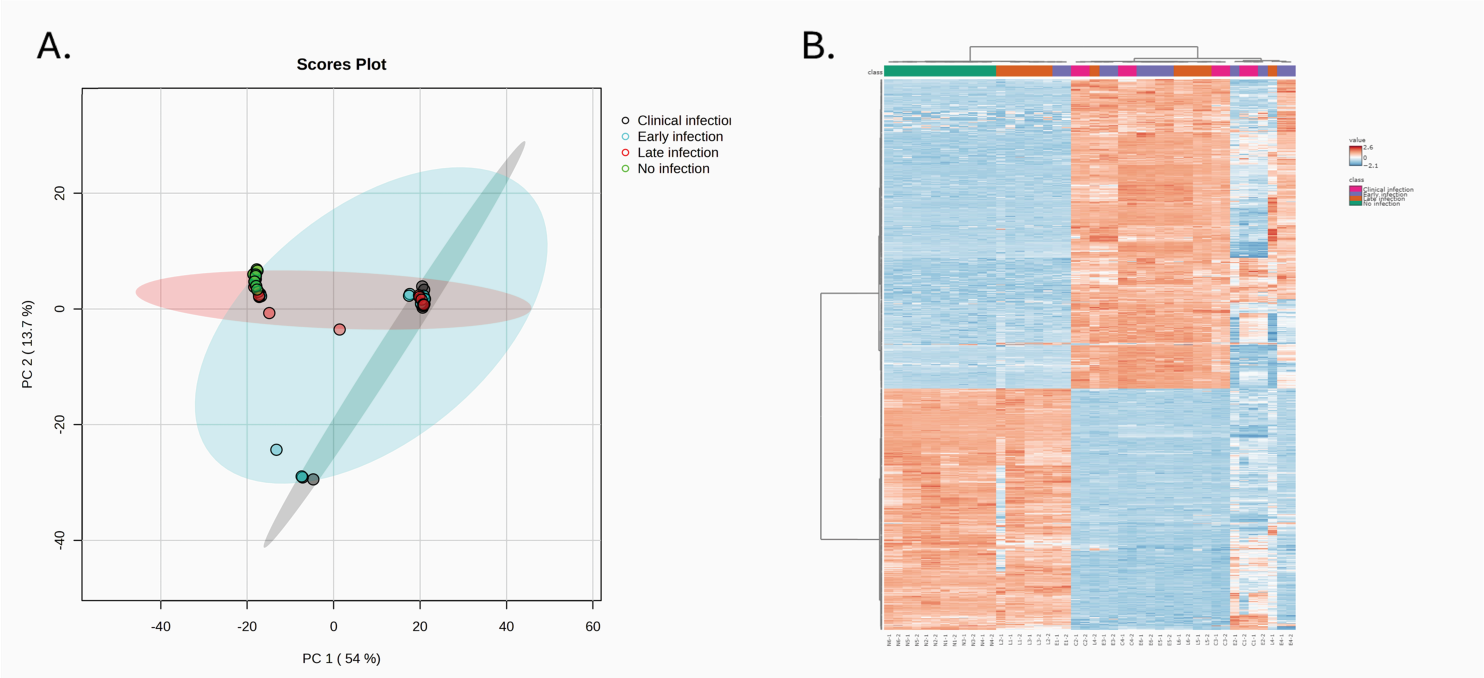


Figure 2

Exploratory data analysis of the metabolomic data. A. The PCA score plot generated from the metabolomic data from all groups. B. The hierarchical clustering heatmap showing the patterns of the metabolomic features.

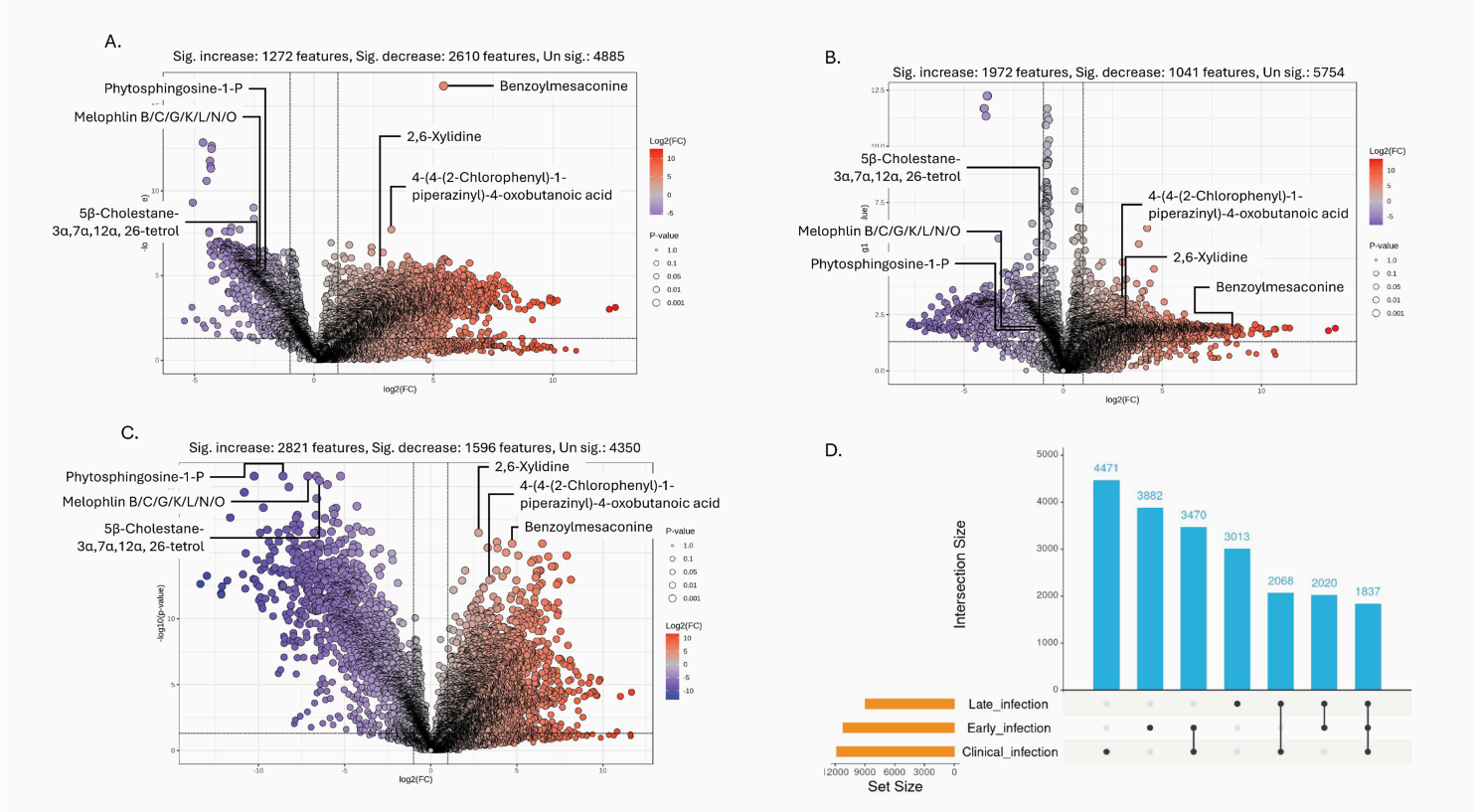


Figure 3

The significantly different serum metabolites that were detected at each stage of RABV infection. A–C. Volcano plots of the serum metabolites detected in the early (A), late (B), and clinical (C) infection groups. D. UpSet plot depicting the overlap among the significantly different metabolites detected at each stage of infection.

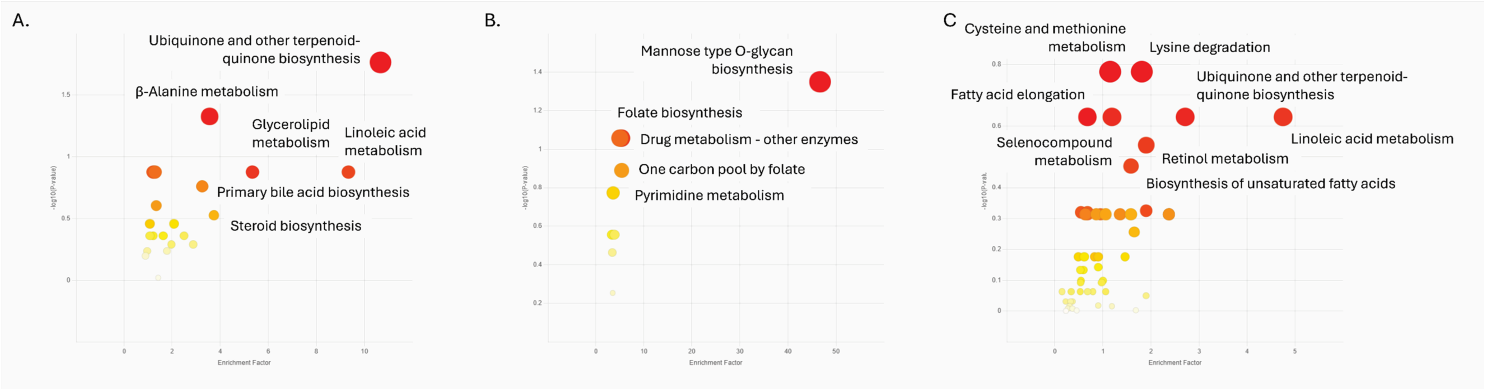


Figure 4

Pathway analysis of significantly different serum metabolites at each stage of RABV infection. A–C. Scatterplots showing the pathways altered in early (A), late (B), and clinical (C) RABV infection.

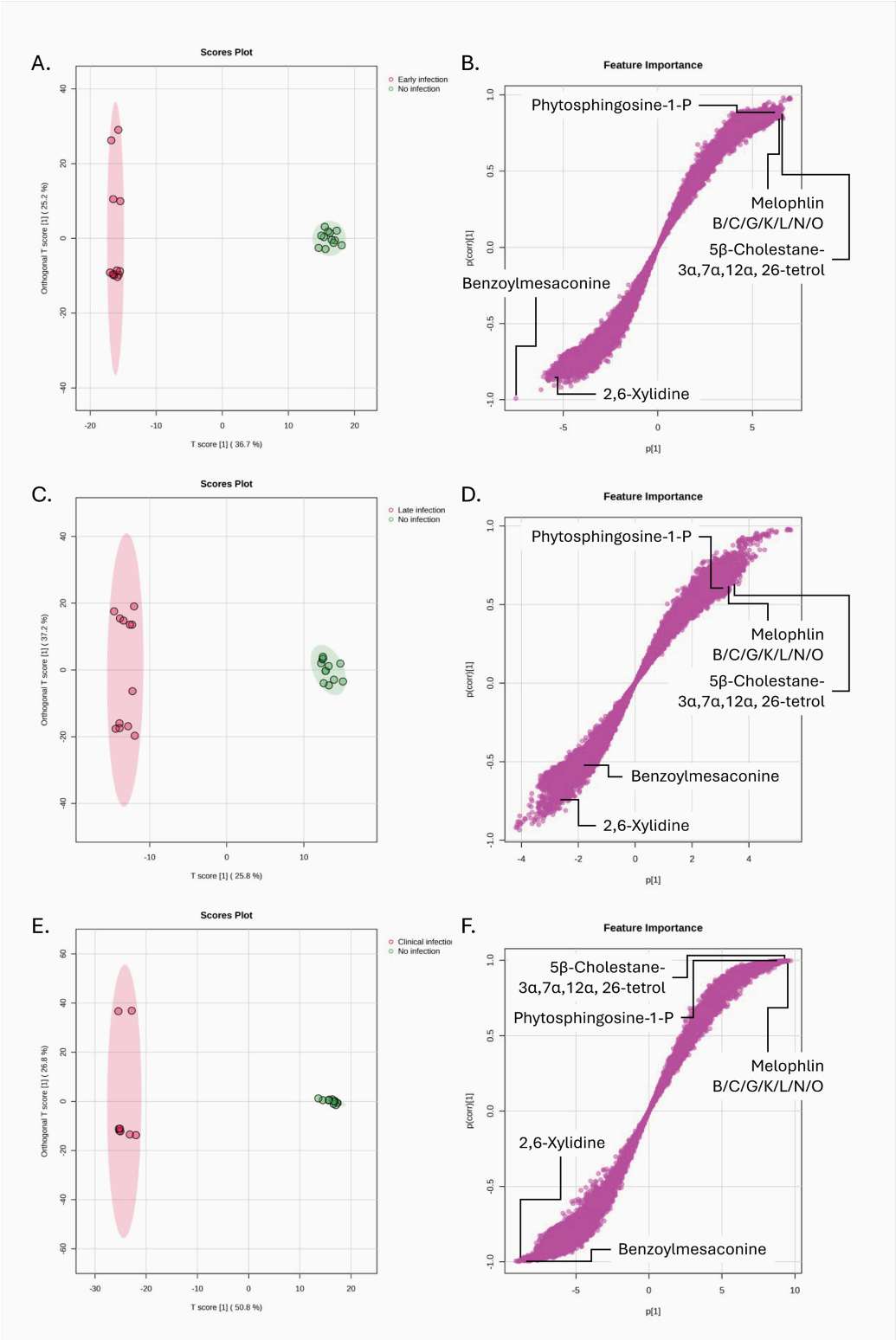


Figure 5

oPLS-DA results for screening of potential biomarkers. A–B. oPLS-DA score plot (A) and S-plot (B) of metabolite features in the early infection group. C–D. oPLS-DA score plot (C) and S-plot (D) of metabolite features in the late infection group. E–F. oPLS-DA score plot (E) and S-plot (F) of metabolite features in the clinical infection group.

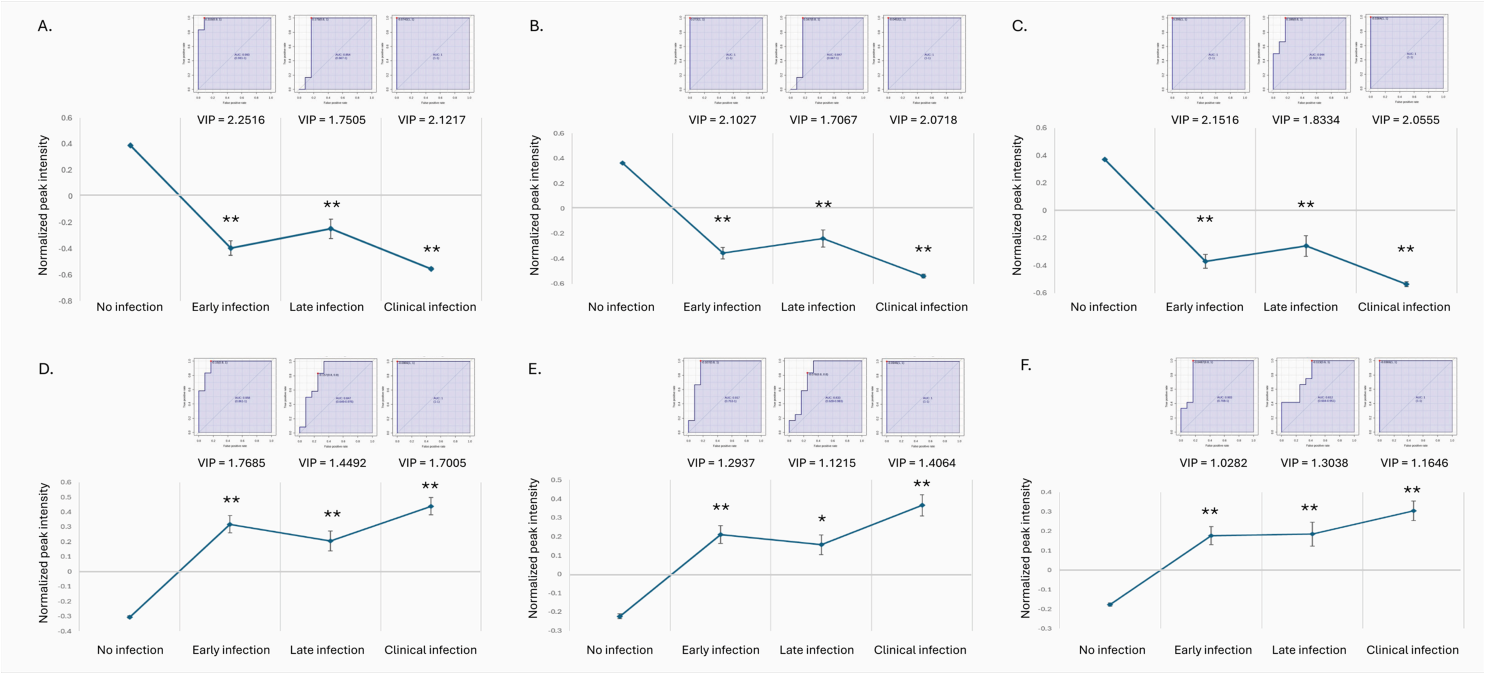


Figure 6

Potential metabolite biomarkers of RABV infection. Normalized peak intensities and AUROC values at all infection stages are shown. A. 5β-Cholestane-3α,7α,12α,26-tetrol. B. Phytosphingosine-1-phosphate. C. 3aH-Cyclopenta[a]chrysene-3a-carboxylic acid, 1-acetyleicosahydro-9-hydroxy-5a,5b,8,8,11a-pentamethyl-, (1R,3aS,5aR,5bR,9S,11aR). D. Cystathionine. E. Glycocholic acid. F. Taurolithocholic acid. * indicates $p < 0.05$. ** indicates $p < 0.01$. Error bars represent standard error.

Supplementary Files

This is a list of supplementary files associated with this preprint. Click to download.

- SupplementarytableS1.xlsx
- SupplementarytableS2.xlsx
- SupplementarytableS3.xlsx
- SupplementarytableS4.xlsx
- SupplementarytableS5.xlsx
- SupplementarytableS6.xlsx
- Supplementaryinformation.pdf